Nature of Crack Path Instabilities in Thin Sheets Cut by Blunt Objects

Eugenio Hamm,[1,*] Iryna Sivak,[2] and Benoît Roman[3]
[1]*Departamento de Física Universidad de Santiago de Chile, Avenida Ecuador 3493, 9170124 Estación Central, Santiago, Chile*
[2]*École Polytechnique Fédérale de Lausanne, CH-1015, Lausanne, Switzerland*
[3]*PMMH, CNRS, ESPCI Paris, Université PSL, Sorbonne Université, Université de Paris, F-75005 Paris, France*

(Received 28 January 2020; revised manuscript received 25 March 2020; accepted 8 April 2020; published 29 April 2020)

Cutting a brittle thin sheet with a blunt object leaves an oscillating crack that seemingly violates the principle of local symmetry for fracture. We experimentally find that at a critical value of a well chosen control parameter the straight propagation is unstable and leads to an oscillatory pattern whose amplitude and wavelength grow by increasing the control parameter. We propose a simple model that unifies this instability with a related problem, namely that of a perforated sheet, where through a similar bifurcation a series of radial cracks spontaneously spiral around each other. We argue that both patterns originate from the same instability.

DOI: 10.1103/PhysRevLett.124.174101

A problem under active development in fracture theory concerns the prediction of the crack path and the associated instabilities: when a piece of material breaks, what determines the shape of the resulting pieces? In this respect, an oscillatory instability occurring in quasistatic propagation of cracks in thermally quenched strips of glass [1] has played an important role in the development of theories for unstable fracture path. Such a simple and clear situation has indeed stimulated a number of studies over the past years [2–5]. Similar instabilities have been observed in oscillatory cracks in stretched rubber [6], drying colloidal films [7], and in the failure of coatings [8], also triggering theoretical developments [9]. In this Letter we analyze two seemingly different crack paths in brittle thin elastic sheets (an oscillatory and a spiral path), and show that they both result from the same instability, by identifying the common control parameter.

When a thin elastic film, clamped along its edges, is cut by a blunt tool displaced parallel to the sheet [configuration $\mathcal{S}$, for *Straight*, in Fig. 1(a)], the expected straight cut is not observed [10–12], but instead an oscillatory path develops along the tool trajectory, breaking the left-right symmetry [Fig. 1(c)]. In a different situation (configuration $\mathcal{C}$, for *Conical*), when a conical tool perforates a brittle sheet [Fig. 1(d)], N cracks may propagate with a radial straight trajectory when $N \geq 4$. But when $N \leq 3$, intertwined spiraling trajectories [13] are observed. Both experiments suggest that the straight path is unstable despite the symmetry of both systems. Previous works focused on the developed patterns, with both geometries correctly captured by a simplified theory for tearing [12–14], but fail in explaining why the straight path is not observed. In this Letter we derive a general framework that captures this feature, and compare its predictions with an experimental setup dedicated to study the instability.

We start by reporting a disregarded experimental fact in previous experiments with configuration $\mathcal{S}$ [Fig. 1(a)]. A rectangular sheet (bioriented polypropylene, thickness

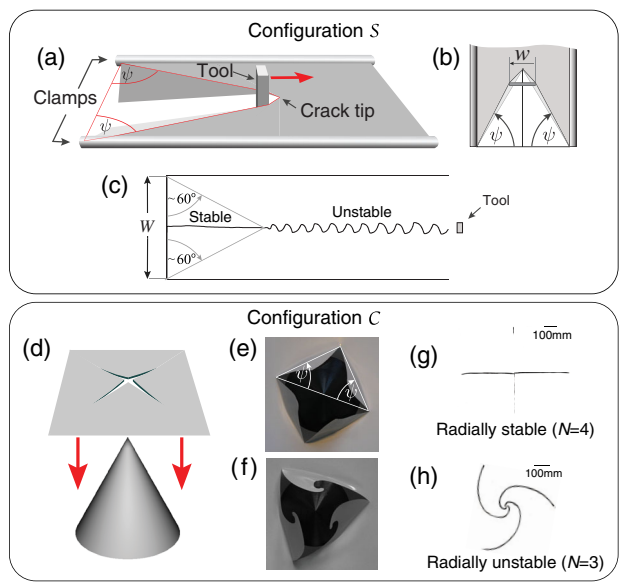

FIG. 1. (a)–(c) Configuration $\mathcal{S}$ and oscillatory crack instability. (a) Setup: a rigid tool of width w with rectangular section is driven along a clamped sheet (width $W \gg w$); (b) upper view: convex hull $\mathcal{H}$ of the cut and the lower edge of the sheet (white region), and material that is stretched due to the pushing tool (clear grey region); (c) scanned crack path for $w = 15$ mm, $W = 155$ mm with a long, straight path before oscillatory instability appears at $\psi \approx 60°$. (d)–(h) Configuration $\mathcal{C}$ and spiral crack instability: (d) a rigid cone is driven across a clamped sheet with $N = 4$ initial radial cuts; (e),(f) ongoing perforations with $N = 4$ (e) and $N = 3$ (f); (g),(h) corresponding scanned crack paths: stable (g) radial path for $N = 4$ and unstable (h) radial path for $N = 3$ leads to three intertwined spiral paths.

 © 2020 American Physical Society

$t = 30\ \mu$m, length 900 mm and width $W = 148$ mm) is clamped along its two long edges and prepared with a centered notch (5 to 10 mm long) on its lower (short) edge. A centered tool with rectangular section of width $w = 15$ mm (the only relevant dimension), is displaced at a constant speed $v = 20$ mm/s, starting from the lower edge and along the midline of the sheet. Attention was previously focused on characterizing the periodic oscillatory regime [10,12,14]. We observe however that in a relatively wide sheet, propagation is first straight, and only becomes oscillatory beyond a certain distance from the lower edge [Fig. 1(b)]. Straight path at the beginning is insensitive to changes in the width, w, of the tool. In this initial regime, the straight path is stable, as evidenced by perturbations relaxing towards the center (this is different from the observation that the instability is suppressed for sufficiently inclined tools [11]). A natural question now arises: under which circumstances is the symmetric (straight) path unstable?

A key concept in tearing [13–15] is the convex hull of the cuts in the sheet because it represents the portion of the sheet that can bend away without generating in-plane stresses. For very thin sheets (with negligible bending stiffness), stresses and fracture propagation may therefore only occur when a tool gets past the boundary of the convex hull. At the early stages of the experiment in configuration $\mathcal{S}$, the convex hull $\mathcal{H}$ is the white triangular region in Fig. 1(b), characterized by an angle ψ at its base. During the experiment, ψ increases continuously as the tool moves forward, up to when the instability develops roughly for $\psi \approx 60°$ [Fig. 1(c)]. We will show that ψ plays the role of a control parameter that locally determines the stability of the straight crack.

We devised a variation of the experiment [configuration $\mathcal{S}'$, Fig. 2(a)] in which we impose a fixed value of ψ, and study the transition from straight to oscillatory propagation, as this control parameter is varied at will. This is achieved by adding a pair of sharp blades on both sides of the sheet, at 2.5 mm from the clamps (separation between blades, 150 mm). The blades move rigidly, together with the tool, keeping angle ψ constant at all times. Experiments show that by increasing ψ, the initially straight path [Fig. 2(b)] becomes oscillatory [Fig. 2(d)] at a critical angle $\psi \approx 56°$ [Fig. 2(c)]. We measure the wavelength λ and the amplitude A of oscillations.

Fracture trajectory can be determined by minimizing at each time the sum of the elastic and fracture energy [16]. If bending energy can be neglected, the elastic membrane energy U is a function of penetration of the tool outside of the convex hull $\mathcal{H}$, which can be defined in terms of the two penetration angles α_l and α_r (here $_{.l,.r}$ refer to left and right, respectively) and corresponding lengths between the pushing point and the crack, l and r [see close-up in Fig. 2(e)]. In previous works [13–15,17] it was assumed that the tool crossed the convex hull boundary only on one side of the

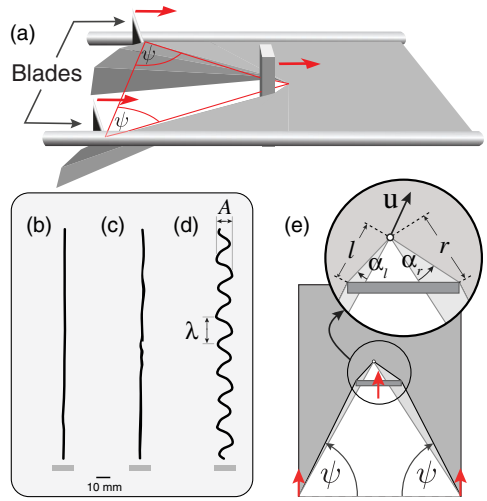

FIG. 2. Configuration $\mathcal{S}'$: modified setup for fixed ψ experiments. (a) Two lateral blades cut the sheet at the same speed as the tool. (b)–(d) Scanned experimental paths for different values of ψ: (b) $\psi = 45°$—straight path, (c) $\psi = 56°$, close to the transition—small humps, (d) $\psi = 66°$—oscillating with measured amplitude (A) and wavelength (λ). Scale is the same on the three cases for comparison. (e) Geometrical parameters of the theoretical model ($\mathbf{u}$ is the propagation direction).

tool [say, the left side as in Fig. 4(a)]. Dimensional analysis then leads to an elastic stretching energy equivalent to

$$U(l, \alpha_l) = aEtl^2 \tan^n \alpha_l, \tag{1}$$

where Et is the two-dimensional stretching modulus (see the Supplemental Material [18] for details). We note that the values of $n = 5$ and 4 introduced previously [14,17] do not change qualitatively the physics, and use here ($n = 3.5, a = 0.0038$) as determined in previous experiments [19]. As the energy U only depends on the position of the crack, the energy release rate (ERR) integrated over the thickness in a direction $\mathbf{u}$ is $G(\mathbf{u}) = [\mathbf{F} \cdot \mathbf{u}]^+$, where $\mathbf{F} = -\nabla U$, and we have noted $[.]^+$, the *positive part*, as $[x]^+ = x$ when $x \geq 0$ and $[x]^+ = 0$ otherwise. Propagation occurs when $G = \gamma t$ (Griffith's criterion), in the direction that maximizes G, hence along vector $\mathbf{F}$, with max $G = \|\mathbf{F}\|$, which is equivalent to minimization of the total energy [16]. The crack trajectory may therefore be determined using these geometrical rules and oscillatory trajectories are well reproduced [12]. When $\gamma/E \ll l$ ($\gamma/E = 4\ \mu$m for the brittle material used in our experiments), fracture occurs [19] for a small penetration angle

$$\alpha_l \approx \left(\frac{\gamma}{anEl}\right)^{\frac{1}{n-1}}. \tag{2}$$

However, this simplified model cannot capture the instability threshold because straight propagation involves simultaneous penetration on both sides of the crack.

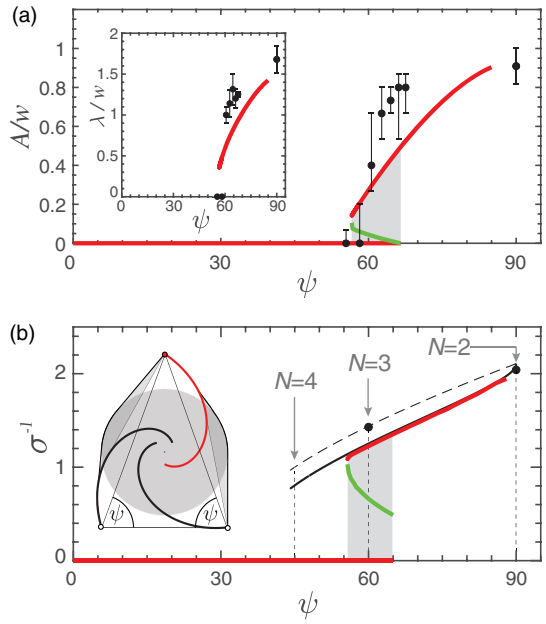

FIG. 3. Bifurcation diagrams for the $\mathcal{S}'$ and $\mathcal{C}$ configurations. (a) Normalized amplitude A/w of the oscillatory crack (black circles). Plotted values correspond to the median over many runs while the error bars indicate the range of measured values ($\psi = 90°$ corresponds to configuration $\mathcal{S}$[10,12]). Green line: threshold of stability for an off-centered initial crack (see text). Inset: mean values of wavelength λ. Error bars correspond to the standard deviation. (b) Inverse of the pitch of spiral (red line) as a function of ψ, as defined in Fig. 1(a). Theoretical prediction for the pitch according to [13] (continuous line) using a penetration angle given by Eq. (2) with $l \approx w/(2\cos\psi)$, and in the limit of vanishing elasticity ($\alpha = 0$, broken line). $N = 2$ and $N = 3$ correspond to experimental values (black circles) taken from [13]. The $N = 4$ spiral is not observable experimentally. Inset: simulated spiral crack (master crack in red, slave cracks in black, pushing cone in grey) with 140°-rotational symmetry (non-commensurate with 2π), corresponding to $\psi = 70°$.

We extend the model to such cases by making the simplistic assumption that the ERR is given by the sum of the independent ERRs of each side of the crack, namely

$$G(\mathbf{u}) = [\mathbf{F}_l \cdot \mathbf{u}]^+ + [\mathbf{F}_r \cdot \mathbf{u}]^+, \tag{3}$$

where $(\mathbf{F}_l, \mathbf{F}_r)$ are the gradients of the left and right elastic energies, according to (1). The crack may be driven only by the left side when $\mathbf{F}_r \cdot \mathbf{u} \leq 0$, only by the right side when $\mathbf{F}_l \cdot \mathbf{u} \leq 0$, or by both sides. We assume that propagation occurs in the direction that maximizes G, when Griffith's criterion is attained.

We numerically solve our enriched model for configuration $\mathcal{S}$, and recover a straight path becoming later oscillatory [as in Fig. 1(c)]. For the modified configuration $\mathcal{S}'$, and despite the simplicity of our assumptions the model predicts the existence of a critical value $\psi_2^{\mathcal{S}} \approx 66.55°$ for the onset of oscillations from an initially centered, straight, longitudinal crack [Fig. 3(a)]. The transition from straight to oscillatory is subcritical though, as evidenced in the numerics by starting from a developed oscillatory pattern with $\psi > \psi_2^{\mathcal{S}}$, and iteratively decreasing ψ while taking at each iteration the developed pattern of the previous iteration as initial condition. This procedure leads to a subcritical threshold $\psi_1^{\mathcal{S}} \approx 56.61°$ below which the oscillations vanish, leading to a straight path. The resulting amplitude and wavelength of the oscillatory pattern are in reasonable agreement with experiments [Fig. 3(a)], without adjusting parameters (we used the same parameters as in an independent experiment [19]). To illustrate the bistability, we consider a particular initial condition, namely a short longitudinal crack, off-centred by a distance δ. We find a marginal curve $\delta_c(\psi)$ [green curve in Fig. 3(a)], with $\psi_1^{\mathcal{S}} < \psi < \psi_2^{\mathcal{S}}$, such that the crack starts oscillating if $\delta > \delta_c(\psi)$, whereas if $\delta < \delta_c(\psi)$ it ends up propagating straight along the midline. The existence of a bistability region was not directly evidenced in experiments, but large fluctuations [see error bars in Fig. 3(a)] were observed close to the threshold. Observing straight propagation beyond $\psi_1^{\mathcal{S}}$, for example for $\psi = 60°$ would require a precision better than 0.7 mm in the initial cut, which is below our experimental error.

In the case of the spiraling instability, we define the control parameter in terms of our initial radial geometry with N cuts as $\psi = \pi/N$ [Fig. 1(e)]. We can however only access discrete experimental values of ψ, because of 2π-rotational periodicity of the plane. Experiments [13] report stable straight paths for $N \geq 4$, which corresponds to $\psi \leq 45°$ whereas radial patterns are unstable for $N \leq 3$, or $\psi \geq 60°$, suggesting a spiraling instability threshold between 45° and 60°. In contrast with experiments, the numerics allow us to artificially impose a rotational symmetry which is not commensurate with 2π, and therefore explore arbitrary values of ψ. In practice we follow the evolution of a crack interacting with two copy versions of itself rotated by 2ψ and -2ψ [see Fig. 3(b), inset]. These slave "copy cracks" are used in the computation of the convex hull to determine the evolution of the center crack. Note that spiral propagation occurs as the tool radius increases continuously, and that the fracture process depends on the system size [for example, in Eq. (2) the penetration angle depends on the size l]. As we wish to compare with the oscillatory case, where the tool has a fixed width w, we maintain in the numerics the spiral to a size comparable to w by artificially rescaling it at each step.

Starting from a set of radial cracks we numerically solve the crack path. We find a critical value $\psi_2^{\mathcal{C}} = 65.1°$ above which a radial path does not exist and leads to a logarithmic spiral path, whose radius increases as $\exp(\sigma\theta)$ (θ is the angle polar coordinate, and σ is the pitch). In this configuration the inverse pitch of the spiral may play the role of an order parameter, since $\sigma^{-1} = 0$ in the radial case and is nonzero for the spiral path. The radial to spiral

bifurcation is also subcritical as can be shown through a continuation method where the pitch of a given spiral is progressively increased (by decreasing ψ). We obtain a critical value $\psi_1^{\mathcal{C}} = 55.65°$ below which no spirals are observed [Fig. 3(b)] for the same parameters as in [19]. The subcritical nature of the transition can be highlighted by taking as initial condition a developed logarithmic spiral of given pitch σ_0 in the range $\psi_1^{\mathcal{C}} < \psi < \psi_2^{\mathcal{C}}$. There exists a critical pitch $\sigma_c(\psi)$ [green line in Fig. 3(b)] such that for any $\sigma_0 > \sigma_c(\psi)$ the radial propagation is recovered while for $\sigma_0 < \sigma_c(\psi)$ a spiral develops. Experimental pitch agree well with the numerics for $\psi = \pi/N$, where N is the number of arms, with $N = 2, 3$ the only possible cases, as predicted ($N = 4$ was however observed [17] in a ductile material).

In configurations $\mathcal{S}'$ and $\mathcal{C}$, the values of α at the critical ψ are not exactly equal, due to geometric differences. We note however that $\psi_1^{\mathcal{C}} \approx \psi_1^{\mathcal{S}}$ and $\psi_2^{\mathcal{C}} \approx \psi_2^{\mathcal{S}}$, confirming that oscillatory and spiral paths originate from the same subcritical instability, and that angle ψ is the single, relevant control parameter for both cases.

Theoretical estimate for ψ_2 (above which a straight solution cannot be observed).—Consider an initially straight, centered crack in a perfectly symmetric situation ($\alpha_l = \alpha_r \doteq \alpha$). In Fig. 5 is plotted the ERR as a function of putative fracture orientation (see the Supplemental Material [18] for analytical expressions). We observe that $G(\mathbf{u})$ generally bears three lobes and three corresponding local maxima (see Fig. 5). The two lateral lobes correspond to propagation only driven by one side (maxima given by $G = \|\mathbf{F}_l\|$ or $\|\mathbf{F}_r\|$), and the central lobe to the case when both sides are active. The critical value ψ_2 corresponds to a propagation equally favourable along the three maximal directions of the ERR. This occurs for $\|\mathbf{F}_l\| = \|\mathbf{F}_r\| = \|\mathbf{F}_l + \mathbf{F}_r\|$, which is only possible if $\mathbf{F}_l$ and $\mathbf{F}_r$ form an angle of 120°. The Griffith criterion requires simultaneously $G = \gamma t$. A calculation valid in the limit of small critical penetration angle $\alpha \ll 1$ gives (see the Supplemental Material [18]) at first order

$$\psi_2 \approx \frac{\pi}{3} + \frac{n-2}{n}\alpha. \tag{4}$$

When $\psi = \pi/3$, an estimate for $\alpha \sim (\gamma/anEw)^{1/(n-1)} \sim 0.2$, which is not a very small number. Equation (4) can therefore only provide a rough estimate, $\psi_2 \sim 65°$, which is however close to our numerical findings (within 2°).

Theoretical estimate for ψ_1 (above which stationary nonstraight solutions exist).—We note that both stationary oscillating and spiraling paths always include a part where the crack tip is "geometrically hidden". By that we mean that one of the penetration angles is zero because the penetration zone is disconnected from the fracture tip as in Fig. 4(a). In such case an incremental crack propagation cannot release energy on the right side, consistently with

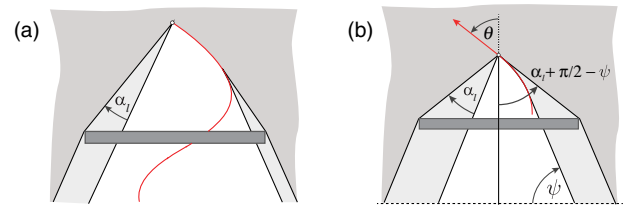

FIG. 4. Hiding mechanism for oscillatory instability. (a) Right pushing point of the tool is hidden from the crack tip: $\alpha_r = 0$; (b) critical condition of hiding for an initially centered crack: $\pi/2 - \psi + \alpha_l = \theta$.

$\mathbf{F}_r = 0$ when $\alpha_r = 0$, and the crack is only driven by the left side.

In configuration $\mathcal{S}'$, the oscillating crack is always hidden when it passes the centerline [as in Fig. 4(a)]. A rough estimate of the subcritical threshold value ψ_1 is obtained when the penetration zone has its outer boundary tangent to the crack path at the crack tip, as sketched in Fig. 4(b) (see also the Supplemental Material [18]). We find that

$$\psi_1 \approx \frac{\pi}{4} + \frac{n-1}{n}\alpha. \tag{5}$$

With $\alpha \approx 0.24$, $\psi_1 \approx 55°$ lies within 2° of numerical values. An identical geometrical construction is obtained for ψ_1 in configuration $\mathcal{C}$, by enforcing that developed spirals always have their crack tips hidden (see the Supplemental Material [18]).

In conclusion, we have unified two very different phenomena observed when fracture of a thin sheet is caused by a blunt object. The oscillatory and spiraling paths both result from the same instability, where the control parameter ψ is a single angle capturing the complex geometry of the cuts and the blunt tool. We were able to impose ψ in a dedicated setup, and also studied theoretically this subcritical instability.

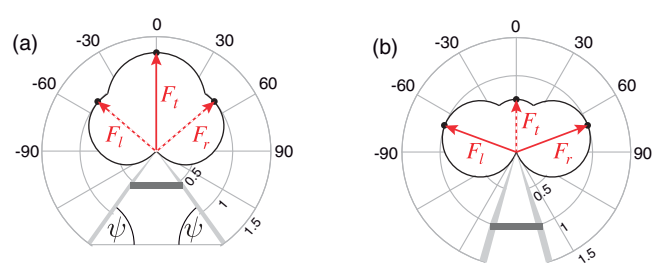

FIG. 5. ERR curves for an initially centered crack. (a) Three-lobed ERR curve for $\psi = 55°$ (below threshold). Local maxima are marked with black dots, according to the global maximum energy release rate criterion, in units of γt. Continuous arrow indicates preferred propagation direction based on the global. (b) Same as (a) but with $\psi = 75°$ (above threshold).

Our results bring some interesting consequences for the cutting of thin films. Since the instability mechanism involves bending of the sheet, which may not occur on lengths comparable to its thickness, an efficient way to impose the cutting path is to use a very sharp blade, with a cutting edge [20] thinner than the sheet [15]. This can become a challenge with ultrathin sheets, as happens with the tearing and perforation of graphene with an atomic force microscopy tip [21,22]. Based on our findings, cutting even with a blunt tool will lead to sharp straight cuts on a distance ℓ if the sheet is held along its edges separated by a width larger than $2\ell/\tan\psi_1$ (the instability is neutralized for $\psi < \psi_1$). We suggest for example that measuring the cutting force along such a regular cut could provide the fracture toughness of ultrathin films, a quantity difficult to obtain from standard metrological methods [22].

I. S. is grateful to Erasmus Mundus for funding her masters in Complex Systems Science. E. H. thanks DICYT 041931HH, Vicerrectoría de lnvestigación, Desarrollo e lnnovación, USACH. B. R. thanks ECOS-CONICYT C12E07 and ANR SMART. We thank A. Fourgeaud for the mechanical design. We also thank the LIA-MSC and the Chaire Joliot (ESPCI) sponsorship.

*luis.hamm@usach.cl

[1] A. Yuse and M. Sano, Nature (London) **362**, 329 (1993).
[2] M. Adda-Bedia and Y. Pomeau, Phys. Rev. E **52**, 4105 (1995).
[3] B. Yang and K. Ravi-Chandar, J. Mech. Phys. Solids **49**, 91 (2001).
[4] F. Corson, M. Adda-Bedia, H. Henry, and E. Katzav, Int. J. Fract. **158**, 1 (2009).
[5] R. D. Deegan, S. Chheda, L. Patel, M. Marder, H. L. Swinney, J. Kim, and A. de Lozanne, Phys. Rev. E **67**, 066209 (2003).
[6] R. D. Deegan, P. J. Petersan, M. Marder, and H. L. Swinney, Phys. Rev. Lett. **88**, 014304 (2001).
[7] L. Goehring, W. J. Clegg, and A. F. Routh, Soft Matter **7**, 7984 (2011).
[8] J. Marthelot, B. Roman, J. Bico, J. Teisseire, D. Dalmas, and F. Melo, Phys. Rev. Lett. **113**, 085502 (2014).
[9] A. A. Leon Baldelli, J.-F. Babadjian, B. Bourdin, D. Henao, and C. Maurini, J. Mech. Phys. Solids **70**, 320 (2014).
[10] A. Ghatak and L. Mahadevan, Phys. Rev. Lett. **91**, 215507 (2003).
[11] P. M. Reis, A. Kumar, M. D. Shattuck, and B. Roman, Europhys. Lett. **82**, 64002 (2008).
[12] B. Roman, P. M. Reis, B. Audoly, S. De Villiers, V. Viguié, and D. Vallet, C. R. Méc. **331**, 811 (2003).
[13] J.-F. Fuentealba, E. Hamm, and B. Roman, Phys. Rev. Lett. **116**, 165501 (2016).
[14] B. Audoly, P.-M. Reis, and B. Roman, Phys. Rev. Lett. **95**, 025502 (2005).
[15] B. Roman, Int. J. Fract. **182**, 209 (2013).
[16] A. Chambolle, G. A. Francfort, and J.-J. Marigo, J. Mech. Phys. Solids **57**, 1614 (2009).
[17] R. Vermorel, N. Vandenberghe, and E. Villermaux, Phys. Rev. Lett. **104**, 175502 (2010).
[18] See the Supplemental Material at http://link.aps.org/supplemental/10.1103/PhysRevLett.124.174101 for details on the theoretical model and its numerical implementation.
[19] V. Romero, B. Roman, E. Hamm, and E. Cerda, Soft Matter **9**, 8282 (2013).
[20] L. Lee, *The Complete Guide to Sharpening* (Taunton Press, Newtown, 1995).
[21] J. Annett and G. L. W. Cross, Nature (London) **535**, 271 (2016).
[22] C. Lee, X. Wei, J. W. Kysar, and J. Hone, Science **321**, 385 (2008).